

# Electrophoresis of a Charge-Inverted Macroion Complex: Molecular Dynamics Study

Motohiko Tanaka<sup>1</sup>, and A.Yu Grosberg<sup>2</sup>

<sup>1</sup>*National Institute for Fusion Science, Toki 509-5292, Japan*

<sup>2</sup>*Department of Physics, University of Minnesota, Minneapolis, MN 55455*

Charge inversion phenomenon of a macroion in a solvent with multivalent salt is studied, applying a constant electric field by molecular dynamics simulations. Interactions of the macroion with surrounding ionic and neutral environment are treated with the explicit use of ions and neutral particles. In a weak electric field, a complex of the macroion drifts with condensed counterions and coions along the electric field, in the direction proving inversion of the charge sign for large Bjerrum length and multivalent counterions. The reversed macroion mobility is insensitive to the applied field, and increases with salt ionic strength. The reversed mobility is maximized at intermediate counterion valence. A very large electric field, comparable to the macroion unscreened field, disrupts charge inversion by stripping the adsorbed counterions off the macroion.

PACS: 61.25.Hq, 82.45.-h, 82.20.Wt

## I. INTRODUCTION

The concept of electrostatic screening has been well known since the work by Debye and Hückel of early 20th century<sup>1</sup>. In recent years, screening by strongly charged ions was found to result in counterintuitive phenomena such as attraction between like-charged macroions<sup>2-5</sup>, and inversion of macroion charges<sup>6-26</sup>. Charge inversion was studied in experiments of colloids and biological materials<sup>6-14</sup>, by analytical theories<sup>16,17,19-22,25,26</sup>, and by Monte Carlo and molecular dynamics (MD) simulations<sup>15,18,23,24</sup>.

Experimentally, the most direct method to observe charged colloids and macroions is electrophoresis. This method is also the prime candidate for the technique of observing charge inversion. However straightforward, this approach causes many questions upon a closer look. Indeed, when an external electric field is applied, does the macroion drift along with its adsorbed multivalent ions? How many multivalent ions are attached to the macroion strongly enough to drift together? How is it affected by the solvent viscosity and the counterflow of monovalent ions? What happens when the field becomes very strong? In other words, what is the field strength sufficient to disrupt the charged complex? These are the fundamental questions necessary to address in order to bridge theoretical concepts of charge inversion and experimental observations.

It should be born in mind that electrophoresis in general has quite a few delicate aspects. Some peculiar ones attracted significant attention recently<sup>17</sup>. The electric field acts not only on the macroions, but on every ion in a solution. In many cases, this leads to effective screening of hydrodynamic interactions which otherwise may be very significant. As the result, complex-shaped particles such as a polymer coil exhibit quite non-trivial behavior in the electric field. This effect can complicate observations of charge inversion of macroions with certain shapes and/or distribution of charges.

One of the difficulties in simulating charge inversion under electrophoresis consists in subtle interactions of

a macroion with surrounding ions and neutral solvent. A naive use of the Langevin equation, assuming that every ion in the system is subject to Stokesian friction  $-6\pi\eta Rv$  and white noise random forces that balance the friction through the fluctuation-dissipation theorem, is hardly justifiable. One counterexample is that, if two spheres are closely located, other particles (either ions or neutral solvent) are excluded from such volume that neither their corresponding frictions nor random forces add to each other. One way of going around this problem is to incorporate macroion-solvent interactions using the Oseen tensor<sup>27</sup>. This is, however, not easy to implement in numerical simulations, because the interactions produce complicated spatial correlations among random forces. Therefore, we address this problem by a direct approach introducing explicit neutral particles to deal with the macroion-salt-solvent interactions in the molecular dynamics simulations.

Our plan in this study is to address electrophoresis of a spherically shaped, uniformly charged macroion, while avoiding the effects that overshadow the phenomenon. We will systematically measure the *net charge* of the drifting macro-ion complex under an external electric field by means of molecular dynamics simulations. We first show that charge inversion takes place on the basis of the net charge for the macroion in solutions containing multivalent counterions due to incomplete screening by coions. The magnitude of reversed mobility of the macroion is found to increase with the salt ionic strength. The reversed mobility is maximized for intermediate valence of the counterions. We also show that a large electric field disrupts the charge-inverted macroion complex and terminates the charge inversion phenomenon.

In this paper, we will confine ourselves to the study of a single macroion interacting with surrounding salt ions and solvent. For the multi-macroion case, a typical run shows that macroions are charge reversed to possess the like-sign charges when the charge inversion onset conditions are satisfied. These macroions tend to exist separately due to mutual repulsions, except for occasional aggregation through collisions forced by strong external

field and/or under dense macroions. Such cases are certainly interesting but beyond the scope of the present paper.

## II. SIMULATION MODEL AND PARAMETERS

We adopt the following model, with  $a$ ,  $e$ , and  $m$  being the units of length, charge and mass, respectively. (We have in mind  $a \sim 2\text{\AA}$  and  $m \sim 40$  a.m.u.) A macroion with negative charge  $Q_0$  between  $-15e$  and  $-180e$  is surrounded by  $N^+$  counterions of a positive charge  $Ze$  and  $N^- \approx 300$  coions of a negative charge  $-e$ . The system is maintained in overall charge neutrality,  $Q_0 + N^+Ze - N^-e = 0$ , which determines  $N^+$  for a given  $Z$ . The mass of the macroion is  $M = 200m$ , and the mass of the co- and counter-ions is  $m$ . We also include  $N_*$  neutral particles with mass  $m/2$ , approximately one particle in every volume element  $(1.5a)^3 \approx (3\text{\AA})^3$  inside the simulation domain, excluding the locations already occupied by the macroion and other ions. These particles are confined in a rectangular box of size  $L = 32a$ , with periodic boundary conditions in all three directions.

In addition to the Coulomb forces, all particles interact through the repulsive Lennard-Jones potential  $\phi_{LJ} = 4\epsilon[(\sigma/r_{ij})^{12} - (\sigma/r_{ij})^6]$  for  $r_{ij} = |\mathbf{r}_i - \mathbf{r}_j| \leq 2^{1/6}\sigma$ , and  $\phi_{LJ} = -\epsilon$  otherwise. Here  $\mathbf{r}_i$  is the position vector of the  $i$ -th particle, and  $\sigma$  is the sum of the radii of two interacting particles, which are chosen as follows: radius of the macroion,  $R_0$ , is between  $3a$  and  $5a$ , counterions and coions have radius  $a$ , and neutral particles  $a/2$ . We relate  $\epsilon$  with the temperature by  $\epsilon = k_B T$ , and choose  $k_B T = e^2/5a$ . The Bjerrum length is thus  $\lambda_B = e^2/k_B T = 5a$ .

Calculation of the Coulomb forces under the periodic boundary conditions involves the charge sum in the first Brillouin zone and their infinite mirror images (the Ewald sum<sup>28</sup>). The sum is calculated with the use of the PPPM algorithm<sup>29,30</sup>. We use  $(32)^3$  spatial meshes for the calculation of the reciprocal space contributions to the Coulomb forces, with the Ewald parameter  $\alpha \approx 0.262$  and the real-space cutoff  $r_{cut} = R_i + 10a$ , where  $R_i$  is the radius of the  $i$ -th ion. A uniform electric field  $E$  is applied in the  $x$ -direction.

When starting the molecular dynamics simulation, we prepare an initial state by randomly positioning all the ions and neutral particles in the simulation domain and giving Maxwell-distributed random velocities corresponding to the temperature  $T_{\text{initial}}$ . We integrate the Newton equations of motion with the use of the leapfrog method<sup>31</sup>, which is equivalent to the Verlet algorithm. In the absence of the electric field ( $E = 0$ ), our system is closed, and its energy is conserved. After an initial transient phase, the distribution of velocities relaxes to a Maxwellian, corresponding to an equilibrium sampling of the microcanonical ensemble. This new Maxwell distribution has the temperature  $T$ , which is a little higher

than  $T_{\text{initial}}$ , because of the release of the potential energy due to screening, i.e., local balancing of charges. We adjust  $T_{\text{initial}}$  such that  $k_B T = \epsilon$ . This makes  $\epsilon$  to be the unique relevant scale of energy, and, accordingly, we put  $\tau = a\sqrt{m/\epsilon}$  as the unit of time. We choose  $\Delta t = 0.01\tau$  as the integration time step. The simulation runs are executed up to  $1000\tau$ .

When an external electric field is present, it performs work on the system; we emphasize that there is no momentum transfer into the system because the system is overall charge-neutral. The corresponding energy, which is Joule heat, is transferred to background neutral particles through collisions with accelerated ions. To simulate an electrophoretic bath that is kept at a constant temperature  $T$ , we refresh the velocities of the neutral particles according to the thermal distribution when they cross the boundaries of the simulation domain, at the center of which the macroion is located at every moment. This procedure maintains temperature stably to within 5%.

There are two possibilities that may quantitatively affect molecular dynamics simulation results described in this paper. One is the finite-size effect of the adopted simulation domain, and the other is the rescaling procedure that could screen hydrodynamic interactions. The former does affect the results, and its scaling is mentioned in Sec.III B. The latter turns out to be not significant by two test runs. First, the mobility obtained by the rescaling procedure described in the last paragraph is found to be within 10% of that obtained without rescaling for weak electric fields  $E \leq 0.3\epsilon/ae$ , for which electrophoresis falls on the linear regime (Sec.III) and thermalization is negligible during the measurement. Second, the rescaling procedure that rescale all neutral particles in every  $100\tau$  time interval yields nearly the same results as above in the linear regime.

## III. SIMULATION RESULTS

### A. General Properties

Our simulation results are shown in Figs.1-7. Figure 1 is a bird's-eye view of (a) all the ions and (b) the vicinity of the macroion. Counterions are shown in light blue and coions in dark blue (neutral atoms are not shown). In this figure, the macroion charge is taken to be  $Q_0 = -30e$ , its radius  $R_0 = 3a$ , counterion valence  $Z = 3$ , and the electric field  $E = 0.3\epsilon/ea$ . It is seen that the macroion is predominantly covered by the counterions. As in the case without the electric field<sup>24</sup>, the radially integrated charge has a sharp positive peak at a distance about  $a$  from the macroion surface. This peak is due to the positive counterions being adsorbed on the macroion surface. The value of the peak charge under the conditions of Fig.1 is  $Q_{\text{peak}} \approx 1.6|Q_0|$ . By contrast, in this paper, we go further to answer whether this is the right index to characterize the charge inversion. Namely, how many counterions and coions drift with the macroion in electrophoresis?

Figure 2 demonstrates the time history of (a) the “peak” charge and (b) the macroion drift speed for the parameters of Fig.1. At time  $t = 10\tau$ , we switch on the external electric field. There is a short transient phase during which a charge-inverted complex is formed through adsorption of counterions to the macroion and condensation of coions on the counterions. This process is reflected in a rather quick rise in  $Q_{\text{peak}}$ , as is shown in Fig.2(a). After the transient phase, we observe a drift of the macroion in the *positive* direction along the applied field. The fact that the drift velocity is positive for the negative bare charge of the macroion ( $Q_0 < 0$ ) is a direct manifestation of charge inversion such that counterions are so strongly bound that they pull the macroion with their motion.

Note that the drift velocity shown in Fig.2(b) is small compared to the thermal velocity  $v_0$  of neutral particles,  $\langle V_x \rangle \sim 0.05v_0$ . Under this condition, exchange of momentum between the macroion and neutral particles is slow, and requires many collisions (compare the similar system in Ref.<sup>33</sup>). Therefore, in terms of hydrodynamics, we are in the linear regime, and expect the average drift speed to be given by the force balance condition,  $Q^*E - \nu V_x \approx 0$ , where  $Q^*$  is the effective charge of the macroion complex and  $\nu$  is the hydrodynamic friction coefficient.

We have measured this friction coefficient in an independent simulation, where we observe an exponential decay of the macroion velocity starting from  $0.5v_0$  for the case without an electric field. We find  $\nu \approx 7.2m/\tau$  for a *neutral* spherical macroion of radius  $R_0 = 3a$ . In reality, the relevant friction is expected to be larger because the macroion drifts by forming a complex with counterions and coions, which contribute to enhance its effective size. A measurement of the friction coefficient for a *fat* macroion with attached co/counterions in the ionic and neutral solvent environment, as is typical during our simulations, yields  $\nu \approx 14.0m/\tau$ .

Using the latter value of the friction coefficient, we obtain the effective charge  $Q^* \approx \nu \langle V_x \rangle / E \approx 5.7e$  for the case of Fig.1. It gives the net charge inversion ratio of  $Q^*/|Q_0| \approx 0.19$ , which is roughly 30% of the maximum inverted charge at the peak of charge distribution,  $(Q_{\text{peak}} - |Q_0|)/|Q_0| \approx 0.6$ . There are two effects contributing to this difference. First, some coions condense on  $Z$ -ions which cuts the net inverted charge. Second, as pointed out in<sup>14</sup>, there is an additional contribution to friction which is due to the counterflow of monovalent coions around the macroion complex. Neither of these factors affects the major qualitative conclusion that the direction of electrophoresis mobility is determined by the inverted charge sign.

Figure 2 also shows significant temporal fluctuations in the drift speed. Inspection reveals that they are larger than what one expects for random kicks of neutral particles. These fluctuations indicate that neither the counterions permanently stick to fixed points on the macroion or the coions attach to the counterions, but that they are

being slowly replaced from time to time. These dynamic fluctuations are indeed seen in a video movie.

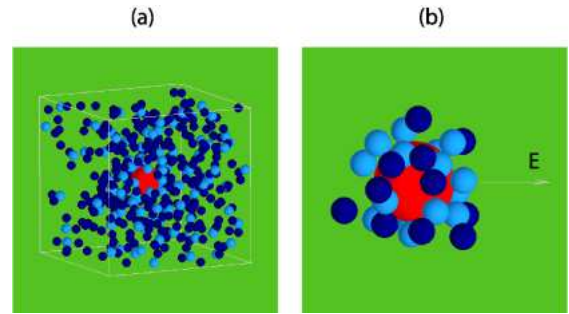


FIG. 1. Bird's-eye view of (a) all the ions in the simulation domain and (b) the screening ion atmosphere within  $3a$  from the macroion surface. A macroion with charge  $Q_0 = -30e$  and radius  $R_0 = 3a$  is the large sphere in the middle; counterions ( $Z = 3$ ) and monovalent coions are shown by light and dark blue spheres, respectively. The arrow to the right shows the direction of the electric field ( $x$ -axis), with  $E = 0.3\epsilon/ea$ .

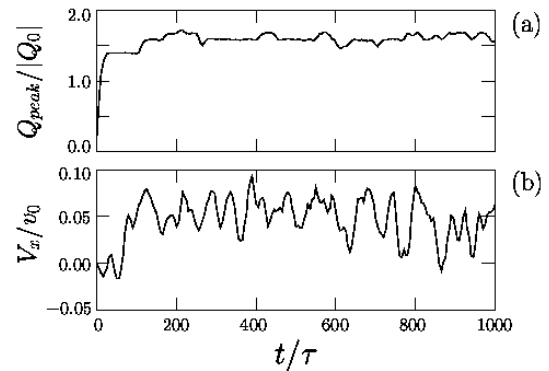


FIG. 2. Time history of (a) the *peak* charge  $Q_{\text{peak}}$  and (b) the macroion speed  $V_x$  normalized by thermal velocity of neutral particles  $v_0$ . The macroion complex drifts positively along the external electric field of  $E > 0$ , which directly indicates the inversion of the charge sign.

## B. Parameter Dependences

### 1. Linear Regime

The dependence of the average macroion drift speed  $V_{\text{drift}}$  on the electric field is shown in Fig.3, where the surface charge densities  $|Q_0|/R_0^2$  for the three series of runs are chosen such that they correspond to the saturation regime in terms of the macroion surface charge density, as will be shown later. We see that the drift speed follows a master curve against the normalized electric field  $ER_0^2/|Q_0|$ .

Let us first discuss the linear drift regime for small electric fields, where  $V_{\text{drift}}$  increases linearly with the field strength. This regime corresponds to the usual Ohm's law. In this regime, the net charge of the complex is

insensitive to the strength of the electric field; a macroion drifts together with its ionic atmosphere as a complex. That is, the electric field is not strong enough to affect the binding of counterions to the macroion. The small electric field regime is characterized by the mobility,  $\mu = \langle V_x \rangle / E$ . If the friction coefficient is assumed to be a constant, the mobility is directly proportional to the net charge of the complex.

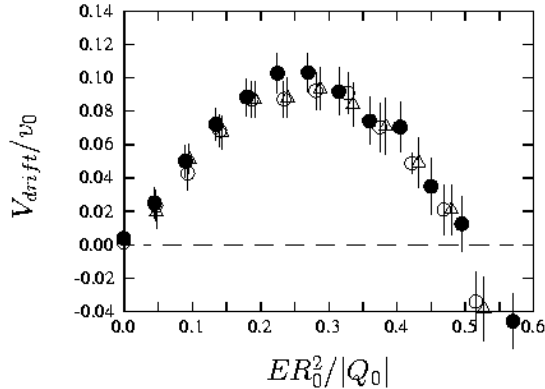


FIG. 3. Dependence of the macroion drift speed  $V_{\text{drift}}$  on the electric field  $E$  for a macroion of various radii:  $R_0 = 3a$  (filled circle),  $R_0 = 4a$  (triangle), and  $R_0 = 5a$  (open circle), where  $v_0$  is thermal speed of neutral particles. The macroion charge is  $Q_0 = -30e$ ,  $-50e$  and  $-80e$  for  $R_0 = 3a$ ,  $4a$  and  $5a$ , respectively, and the valence of counterions is  $Z = 3$ .

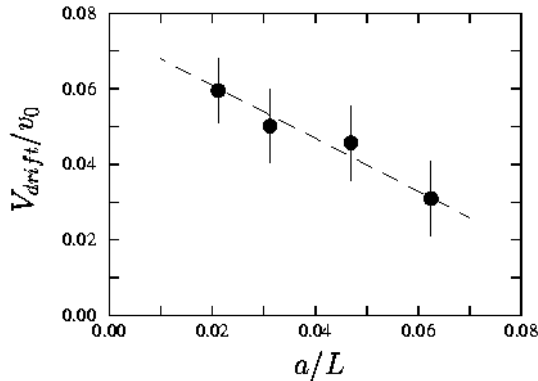


FIG. 4. Effect of the finite domain size  $L$  on the drift speed  $V_{\text{drift}}$  for a macroion with  $R_0 = 3a$ ,  $Q_0 = -30e$ , and the electric field  $E = 0.3e/a$ .

Throughout this paper, we choose the simulation system of a periodic cube of the length  $L = 32a$ . Since hydrodynamic interactions are of the long range, it is beneficial to find the corrections due to the finite domain size. Figure 4 shows the finite-size effect of the simulation domain  $L$  on the macroion mobility. By a series of the runs with different simulation domain sizes and under fixed neutral density and salt ionic strength, we have confirmed that the finite domain-size correction is proportional to  $-a/L$ , in agreement with the case of

polymer chains<sup>32</sup>. More specifically, we have obtained  $V_{\text{drift}}/v_0 \cong 0.075 - 0.7a/L$  for the parameters of Fig.3 ( $E = 0.3e/a$  and  $R_0 = 3a$ ). Therefore, the mobility and, hence, the net charge of a macroion placed in an infinite volume is about 40% larger than that for the case with  $L = 32a$  cube.

Figure 5 shows the dependence of mobility on the surface charge density of the macroion  $|Q_0|/R_0^2$  for the macro- ion radii  $R_0 = 3a$  and  $5a$ . The macroion charge  $Q_0$  is varied between  $-15e$  and  $-70e$  for  $R_0 = 3a$ , and between  $-30e$  and  $-180e$  for  $R_0 = 5a$ . There appears to be a minimum charge density for charge inversion to take place. The reversed mobility first increases linearly for small surface charge densities  $|Q_0|a^2/eR_0^2 \leq 3$ . A half the separation of two counterions (the Wigner cell radius) on the macroion surface is roughly  $2a$  at  $|Q_0|/R_0^2 \sim 3e/a^2$ . Above this value, the mobility becomes nearly insensitive to the surface charge density. The linear regime is similar to our previous observations for the peak inverted charge<sup>24</sup>. The saturation regime is attributed to neutralization such that any new addition of counterions to the complex is exactly compensated by newly condensed coions.

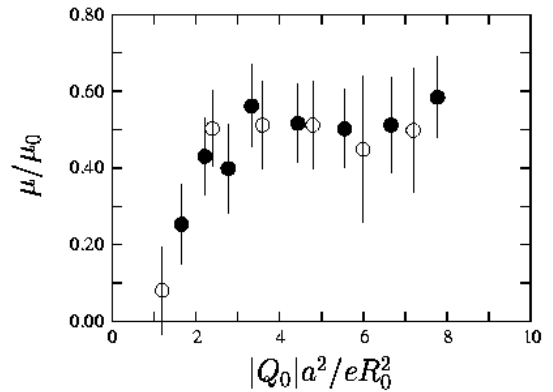


FIG. 5. Dependence of the macroion mobility  $\mu$  on the surface charge density  $Q_0/R_0^2$  for  $R_0 = 3a$  (filled circle) and  $R_0 = 5a$  (open circle). Here,  $\mu_0 = v_0/(|Q_0^{(0)}|/(R_0^{(0)})^2)$  with  $Q_0^{(0)} = -30e$  and  $R_0^{(0)} = 3a$ . The parameter are the valence  $Z = 3$ , the electric field  $E = 0.3e/a$ , and the temperature  $e^2/ak_BT = 5$ .

The dependence of the macroion mobility  $\mu$  on the valence of the counterions  $Z$  in Fig.6 is physically interesting, and also important for application purposes. For the cases shown with filled and open circles, the surface charge density of the macroion  $|Q_0|/R_0^2$  is chosen nearly the same so that they reside in the saturation regime of Fig.5. We emphasize that the mobility for these cases is given by a unique curve, which is *negative* for monovalent counterions  $Z = 1$ , due to the normal Debye screening. Thus, the charge inversion phenomenon does not occur in the solution of monovalent salt if the co- and counterions have the same radii. For  $Z \geq 2$ , charge inversion does take place, as manifested by the *positive* mobility.

These observations agree with a previous study for planar charged surfaces<sup>19</sup>. A remarkable finding is that the mobility here is maximized for an intermediate valence,  $Z \approx 4$ , unlike the peak inverted charge that counts static charge distribution of mainly counterions<sup>24</sup>.

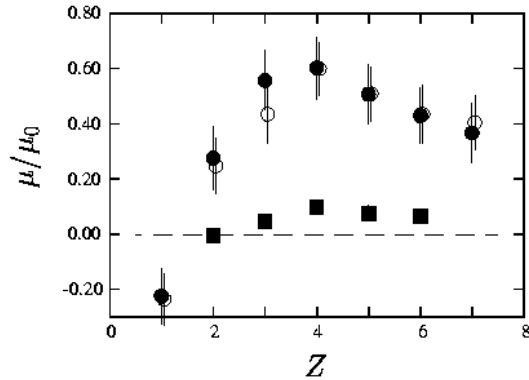


FIG. 6. Dependence of the macroion mobility  $\mu$  on the valence of the counterions  $Z$  for three series of the runs:  $R_0 = 3a$  and  $Q_0 = -30e$  (filled circle),  $R_0 = 5a$  and  $Q_0 = -80e$  (open circle), and  $R_0 = 5a$  and  $Q_0 = -40e$  (square). Here,  $\mu_0 = v_0/(|Q_0^{(0)}|/(R_0^{(0)})^2)$  with  $Q_0^{(0)} = -30e$  and  $R_0^{(0)} = 3a$ . The external electric field is  $E = 0.3\epsilon/ae$ .

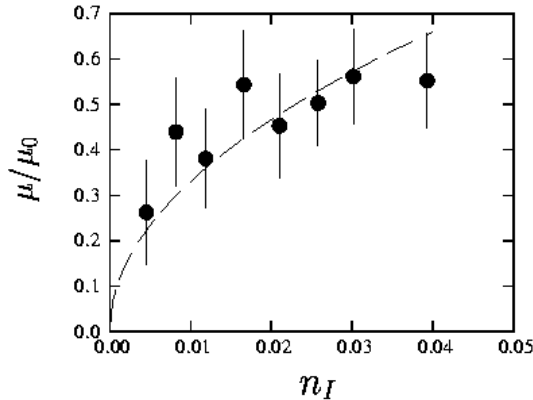


FIG. 7. Dependence of the macroion mobility  $\mu$  on the salt ionic strength,  $n_I = (Z^2 N^+ + N^-)/L^3$ . The parameters are  $Q_0 = -30e$ ,  $R_0 = 3a$ ,  $E = 0.3\epsilon/ae$ ,  $Z = 3$  and  $e^2/ak_B T = 5$ , which yield  $a/\lambda_D \sim 0.79$  for  $n_I = 0.01$  with  $\lambda_D$  the Debye length.

It is also noted that, when the surface charge density is reduced to a half, the regime and magnitude of reversed (positive) mobility shrink as shown by square symbols in Fig.6. The mobility for  $Z = 2$  is now negative. This happens because these parameters yield small surface charge density  $Q_0/R_0^2$ , corresponding to the linear slope regime in Fig.5. Yet, the mobility is maximized around the valence  $Z \cong 4$ . These results of macroion mobility with respect to the counterion valence are in line with the electrophoretic mobility measurement of nucleosome core particles in cation solution<sup>14</sup>. There, the observ-

able range in the cation concentration and magnitude of reversed mobility increased when spermidine (+3) was replaced with spermine (+4), while charge reversal was not observed for any concentration of  $Mg^{+2}$ .

The presence of an optimum valence for the reversed mobility in Fig.6 is explained in the following manner. First, large valence is favorable for charge inversion because of strong Coulomb correlations among counterions. Second, on the other hand, the iso-potential surfaces produced by a macroion plus "surface" counterions are found to become very rugged (anisotropic) as the valence becomes large; small number of clear three-dimensional potential holes appear since the surface counterions make large correlation holes on the macroion. Competition of these two mechanisms causes the optimum valence for the macroion mobility. This mechanism also applies to the mobility in the regime of small surface charge density of Fig.5, where the ion correlation holes on the macroion are again large.

The dependence of the macroion mobility on the salt ionic strength,  $n_I = (Z^2 N^+ + N^-)/L^3$  is shown in Fig.7 for the counterion valence  $Z = 3$  and the temperature  $e^2/ak_B T = 5$ . Here, the ionic strength is related to the Debye length  $\lambda_D$  by  $\lambda_D/a = (k_B T/4\pi n_I e^2)^{1/2}$ . The mobility increases quite rapidly for small ionic strength, and is well fit by  $\mu \propto n_I^{1/2}$  as shown by a dashed curve. The quick rise in the reversed mobility at small ionic strength agrees with the colloidal mobility measurement for the trivalent salt  $LaCl_3$ <sup>8,16</sup>.

## 2. Nonlinear Regime

Let us now return to Fig.3 to discuss the regime that is nonlinear in the applied electric field. As the figure indicates, the charge-inverted shell around the macroion is destroyed for large electric fields. Moreover, the critical field  $E_c$  at which this happens is independent of the macroion size, which leads us to an estimate

$$E_c \approx 0.5|Q_0|/R_0^2. \quad (1)$$

This result is quite interesting. Indeed,  $|Q_0|/R_0^2$  is the electric field on the macroion surface produced by the macroion bare charge. Why does the critical field scale with the bare charge of the macroion instead of the net charge of the complex? The reason is due to correlations between screening ions. We noted while discussing Fig.2 that the counterions on the macroion surface are being replaced from time to time. Consider how one  $Z$ -ion can depart from the macroion surface. Since this ion is surrounded by a correlation hole on the surface, its departure requires work against the unscreened bare electric field of the macroion as long as its distance from the surface is smaller than the distance between the adsorbed  $Z$ -ions. Therefore, departure from the surface becomes possible when the external field becomes com-

parable with this unscreened field; the charge-inverted complex is no longer stable at such a field strength.

The critical electric field in realistic situations is estimated to be very large. For the parameters  $R_0 \approx 20\text{\AA}$  and  $Q_0 \approx 30e$ , the critical electric field becomes as large as  $E_c \approx 0.5Q_0/\epsilon R_0^2 \approx 67\text{V}/\mu\text{m}$ , where we took into account the dielectric constant of water  $\epsilon \approx 80^{34}$ . Although the critical field is large, it gives small energy to the electric dipole of a water molecule,  $d \approx 2 \times 10^{-18}\text{esu} \cdot \text{cm}$ :  $E_c d/k_B T \sim 0.11 < 1$ . This verifies the use of the model solvent of neutral particles in the present molecular dynamics simulations. In practice, the applied electric field is not expected to disrupt the charge-inverted macroion complex.

#### IV. SUMMARY

In this paper, we adopted the electrophoresis and neutral-particle solvent in molecular dynamics simulations, and measured the drift speed of a macroion to obtain its mobility in a multivalent salt solution.

A weak electric field did not disrupt the macroion complex, but pulled it in the direction determined by the net inverted charge. The reversed mobility of the macroion complex,  $\mu = V_{\text{drift}}/E$ , was shown to be nearly constant against weak electric fields. We showed that the mobility is represented by three master curves in Figs.3, 5 and 6 of Sec.III, respectively, against the electric field strength  $E$ , the surface charge density of the macroion  $Q_0/R_0^2$ , and the valence  $Z$  of the counterions, irrespectively of different macroion radii and charges. The reversed mobility increased rapidly with the salt ionic strength  $n_I$  as  $\mu \propto n_I^{1/2}$ .

It was interesting that the reversed mobility was maximized for the intermediate valence of the counterions. Also, the mobility increased linearly for small surface charge density  $|Q_0|a^2/eR_0^2 \leq 3$ , above which the mobility became insensitive to the surface charge density. These dependences were explained by the competition of strong correlations among the macroion and counterions, and the presence of few three-dimensional potential holes as the valence increased; either of these conditions leads to large correlation holes of counterions on the macroion surface.

In the large field regime, although academic because of its huge value, electrophoresis was strongly nonlinear, and the field stripped the screening counterions off the macroion. The mobility of the macroion complex dropped significantly from that of the linear regime, and the sign of the mobility flipped back to non-reversed one above the critical electric field, which was approximately half the macroion *unscreened* field.

#### ACKNOWLEDGMENTS

The authors are grateful to Professor B.Shklovskii and Dr.T. Nguyen for discussions, and to Dr.J.W.Van Dam for reading the manuscript. One of the authors (M.T.) thanks Professor K.Kremer and Dr.C.Holm for collaboration on the PPPM algorithm during his stay at the Max-Planck Institut für Polymerforschung (Mainz, 1999) under the support of the Max-Planck Society. The numerical computation was performed with the vpp800/12 of the Institute of Space and Astronautical Science (Japan) and partly with the Origin 3800 of the University of Minnesota Supercomputing Institute.

- <sup>1</sup> P. Debye and E. Hückel, *Phys.Zeitsch.* **24**, (1923) 185.
- <sup>2</sup> J.C.Crocker and D.G.Grier, *Phys.Rev.Lett.* **73**, (1994) 352.
- <sup>3</sup> I. Rouzina and V. A. Bloomfield, *J.Phys.Chem.* **100**, (1996) 9977.
- <sup>4</sup> P.Linse and V.Lobaskin, *Phys.Rev.Lett.* **83**, (1999) 4208.
- <sup>5</sup> T.Squires and M.Brenner, *Phys.Rev.Lett.* **85**, (2000) 4976.
- <sup>6</sup> H.G. Bungenberg de Jong, *Colloid Science, vol.2*, edited by H.R. Kruyt (Elsevier, 1949) 259-330.
- <sup>7</sup> U.P.Strauss, N.L.Gershfeld, and H.Spiers, *J.Amer. Chem. Soc.* **76**, (1954) 5909.
- <sup>8</sup> M.Elimelch, and C.R.O'Melia, *Colloids Surf.* **44**, (1990) 165.
- <sup>9</sup> J.Xia and P. L. Dubin, *Macromolecular complexes in Chemistry and Biology*, edited by P.L.Dubin et al. (Springer-Verlag, Berlin, 1994).
- <sup>10</sup> A.V.Kabanov, and V.A.Kabanov, *Bioconjug. Chem.* **6**, (1995) 7.
- <sup>11</sup> H.W. Walker and S.B. Grant, *Colloids and Surfaces A* **119**, (1996) 229.
- <sup>12</sup> A.V.Kabanov, and V.A.Kabanov, *Advanced Drug Delivery Reviews* **30**, (1998) 49.
- <sup>13</sup> H.M. Evans, A. Ahmad, T. Pfohl, A. Martin and C.R. Safinya, *Bull.APS* **46**, (2001) 391.
- <sup>14</sup> M.de Frutos, E.Raspaud, A.Leforestier, and F.Livalant, *Biophys.J.* **81**, (2001) 1127.
- <sup>15</sup> W.van Mengen, and I.Snook, *J.Chem.Phys.* **73**, (1980) 4656.
- <sup>16</sup> E.Gonzales-Tovar, M.Lozada-Cassou, and D.J. Henderson, *J. Chem.Phys.* **83**, (1985) 361.
- <sup>17</sup> D.Long, J.Viovy, and A.Ajdari, *Phys.Rev.Lett.* **76**, (1996) 3858.
- <sup>18</sup> L.Sjostrom, T.Akesson and B.Jonsson, *Ber.Bunsenges. Phys.Chem.* **100**, (1996) 889.
- <sup>19</sup> H.Greberg, and R.Kjellander, *J.Chem.Phys.* **108**, (1998) 2940.
- <sup>20</sup> B.I.Shklovskii, *Phys.Rev.E* **60**, (1999) 5802.
- <sup>21</sup> T.T.Nguyen, A.Yu. Grosberg and B.I. Shklovskii, *Phys. Rev. Lett.* **85**, (2000) 1568.
- <sup>22</sup> F.J.Solis, and M.Olvera de la Cruz, *J.Chem.Phys.* **112**, (2000) 2030.

- <sup>23</sup> R.Messina, C.Holm and K.Kremer, *Phys.Rev.Lett.* **85**, (2000) 872.
- <sup>24</sup> M.Tanaka and A.Yu. Grosberg, *J.Chem.Phys.* **115**, (2001) 567.
- <sup>25</sup> M.Lozada-Cassou, E.Gonzales-Tovar, and W.Olivares, *Phys.Rev. E* **60**, (1999) R17; M.Lozada-Cassou and E.Gonzales-Tovar, *J.Colloid Interf.Sci.* **239**, (2001) 285.
- <sup>26</sup> A.Yu. Grosberg. T.T. Nguyen, and B.I. Shklovskii, *cond-mat/0105140*.
- <sup>27</sup> L.D. Landau and E.M. Lifshitz, *Theoretical Physics, vol. 6, Fluid Mechanics* (Butterworth-Heinemann, 1990).
- <sup>28</sup> P.P.Ewald, *Ann.Physik* **64**, (1921) 253.
- <sup>29</sup> J.W.Eastwood and R.W.Hockney, *J.Comput.Phys.* **16**, (1974) 342.
- <sup>30</sup> M.Deserno and C.Holm, *J.Chem.Phys.* **109**, (1998) 7678.
- <sup>31</sup> D.Frenkel and B.Smit, *Understanding Molecular Simulation* (Academic Press, 1996)
- <sup>32</sup> B.Dünweg, *J.Chem.Phys.* **99** (1993) 6977.
- <sup>33</sup> E.M.Lifshitz and L.P.Pitaevskii, *Theoretical Physics, vol. 10, Physical Kinetics* (Butterworth-Heinemann, 1981).
- <sup>34</sup> I.Ohmine and S.Saito, *Accounts Chem. Res.* **32**, (1999) 741.